Experimental Report

25/01/2013

Proposal:	**4-01-1232**	**Council:**	4/2012	
Title:	Dispersion of low-energy resonant spin excitations in CeB6			

This proposal is a new proposal

Researh Area: Physics

Main proposer: **INOSOV Dmytro**

Experimental Team: NASSAR Roy
JANG Hoyoung
INOSOV Dmytro
FRIEMEL Gerd
PORRAS PEREZ GUERRERO Juan Pablo

Local Contact: OLLIVIER Jacques

Samples: CeB6 (99.7% enriched with 11B)

Instrument	Req. Days	All. Days	From	To
IN5	10	7	29/10/2012	05/11/2012

Abstract:

Among the RB6 family of hexaborides (R being a rare earth), CeB6 stands out as the only compound that exhibits an exotic ordered phase in the narrow temperature range between TN = 2.3 K and TQ = 3.2 K, commonly referred to as the antiferroquadrupolar (AFQ) phase or “phase II”. Its true nature is not yet fully understood and is discussed controversially. In our recent experiments performed at IN14, we have discovered a strong magnetic “exciton” mode at the AFQ wavevector
R(1/2,1/2,1/2), setting in below the antiferromagnetic ordering temperature, TN, and an ellipse-shaped structure of weaker intensity lobes that connect equivalent R points [1]. In the present proposal, we suggest to map out the full energy-momentum space with high energy resolution on the same sample, using time-of-flight spectrometer IN5, in order to investigate the full 3D momentum structure of the newly discovered excitations and their energy dependence.

Experimental report for proposal No. 4-01-1232

Introduction

The heavy-fermion metal CeB_6 shows two successive low-temperature phase transitions, associated with an antiferromagnetic (AFM) order ($T_N = 2.3$ K) and an antiferro-quadrupolar (AFQ) order ($T_Q = 3.2$ K) [1], as shown in Fig. 1. The AFQ order (phase II) can be observed directly by resonant x-ray diffraction [2, 3], but is generally believed to be invisible to neutron scattering [4] unless an external magnetic field is applied [1]. Therefore, it is sometimes referred to as a *magnetically hidden order*. However, more recent experiments revealed a weak magnetic Bragg peak at the AFQ wave vector in zero field [5, 6], which could indicate a deviation from this commonly accepted model or the presence of a separate coexisting order parameter at the same wave vector. In our previous inelastic neutron scattering (INS) experiments performed using the IN14 triple-axis spectrometer (TAS) at the ILL, we have discovered a strong magnetic exciton mode at the AFQ wavevector $R(\frac{1}{2}\frac{1}{2}\frac{1}{2})$, setting in below T_N, and an additional ellipse-shaped structure of weaker intensity lobes that connect equivalent R points [6, 7]. The goal of the present IN5 experiment was to map out the full 3D momentum structure and dispersion of these low-energy excitations on the same sample with high energy resolution by means of the cold-neutron time-of-flight spectroscopy.

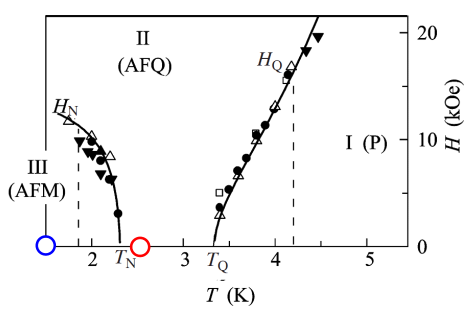

Fig. 1: H–T phase diagram of CeB_6 [9]. Circles mark the experimental conditions of our IN5 experiment.

Experimental configuration

For this experiment, we used a large cylindrical single crystal of $Ce^{11}B_6$ with a mass of ~ 4 grams, prepared from 99.6% isotopically enriched ^{11}B to minimize neutron absorption. CeB_6 has a simple cubic crystal structure with the lattice constant 4.14 Å. The sample was mounted in the cryostat with its crystallographic $\langle 1\bar{1}0\rangle$ axis aligned vertically, so that the sample rotation axis went nearly parallel to the axis of the cylindrical crystalline rod. The incident neutron wavelength was fixed at 5 Å (3.27 meV), so that the energy transfer up to 2 meV could be reached. The corresponding energy resolution was sufficiently good to resolve the inelastic signal down to 0.1 meV energy transfer without any contamination from the elastic line. The sample was rotated during the measurement in steps of 0.5° to map out the complete energy-momentum space in 4D. The counting time per every sample position was ~ 20 min or more. We have performed all measurements in the absence of magnetic field at two temperatures, $T = 1.5$ K (AFM phase) and $T = 2.6$ K (AFQ phase), as indicated by blue and red circles in Fig. 1 (a). We could not obtain a reference measurement at a higher temperature due to limited beam time.

4D energy-momentum space mapping

In the following, we will present several representative cuts from the 4D datasets acquired in this experiment to illustrate the quality of the data and our main results. Fig. 2 shows (HHL) and $(H+\frac{1}{8}\ H-\frac{1}{8}\ L)$ inelastic intensity maps at various energies both in the AFM and AFQ states. At 0.5 meV [panel (c)], the data are in agreement with the corresponding *FlatCone*

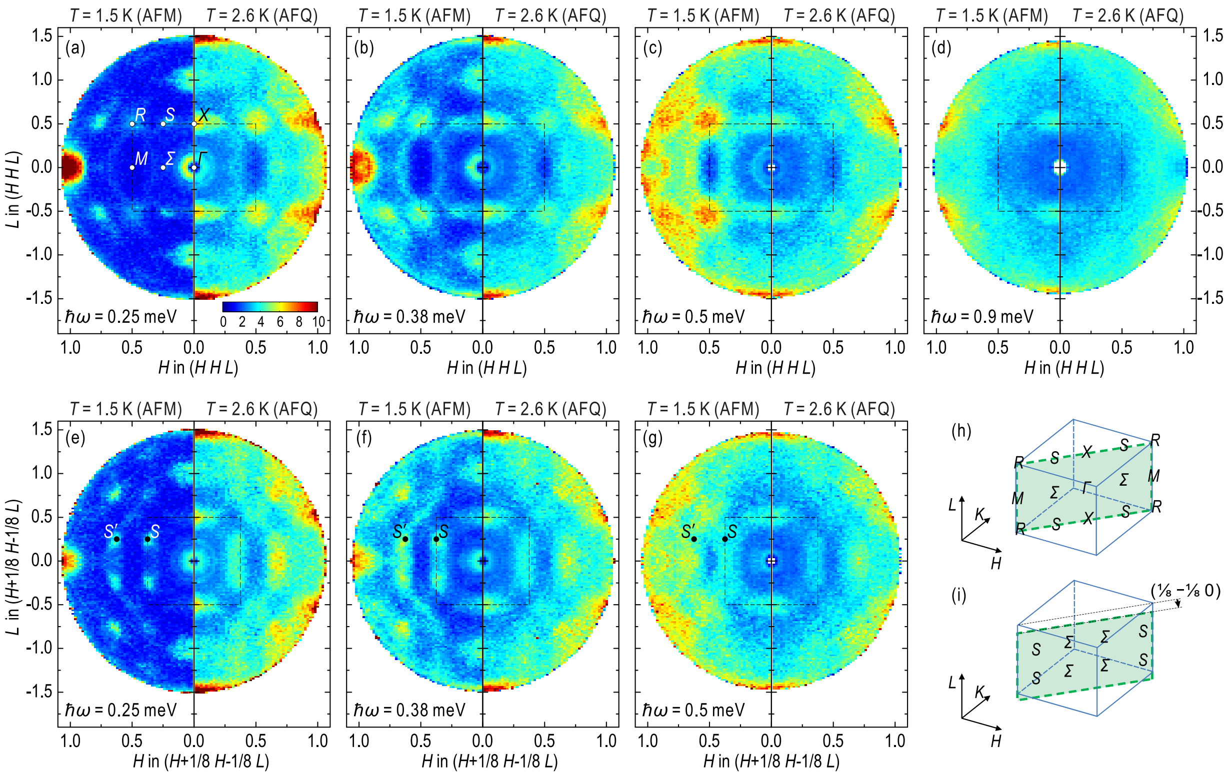

Fig. 2: (a)–(d) (HHL) maps at $\hbar\omega = 0.25$, 0.38, 0.5, and 0.9 meV. (e)–(g) $(H+\frac{1}{8}\ H-\frac{1}{8}\ L)$ maps at $\hbar\omega = 0.25$, 0.38, and 0.5 meV. The data were symmetrized with respect to the natural mirror planes of the reciprocal space. The left and right halves of every panel show the data in the AFM and AFQ states, respectively. (h, i) The (HHL) and $(H+\frac{1}{8}\ H-\frac{1}{8}\ L)$ reciprocal-space planes with high-symmetry points.

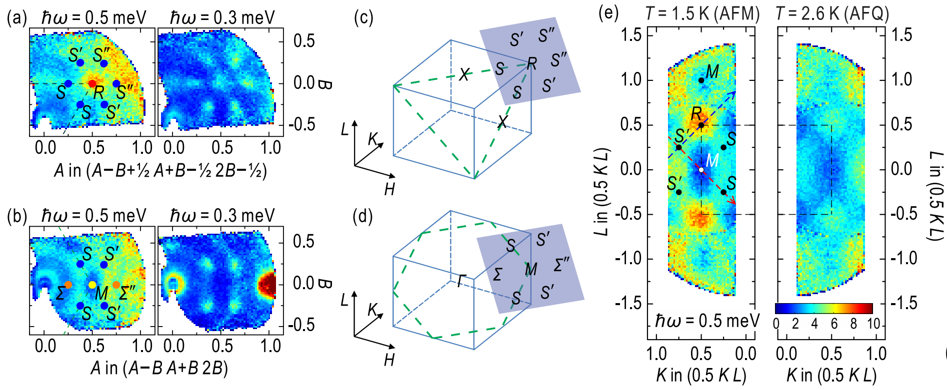

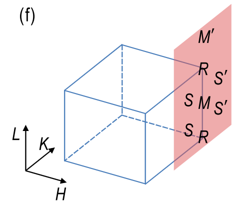

Fig. 3: (a, b) Low-temperature ($T = 1.5$ K) inelastic intensity maps normal to the $(1\bar{1}\bar{1})$ vector and crossing R and M points, respectively. (c, d) Sketches of the respective planes in the reciprocal space. (e, f) The same for the $(\frac{1}{2}KL)$ plane.

map obtained previously at IN14 [6], confirming the presence of an intense exciton mode at the R point in the AFM phase, which is considerably suppressed above T_N. At a higher energy of 0.9 meV [panel (d)], we also observe the second excitonic mode seen previously in the TAS data [6]. Here we can clearly see the elliptical cross section of this mode. In addition, we also observe conventional spin-wave excitations at lower energies emanating from the AFM Bragg-peak positions at the S and Σ points [panels (a), (b), (e), (f)], which have a much weaker intensity. By following their evolution as a function of energy, we come to the conclusion that the elliptical feature surrounding the M point is most likely originating from the top of the multiple spin-wave branches, which coincides in energy with the exciton mode. The most striking new feature in our dataset is a very intense mode centered at the Γ point (ferromagnetic wave vector) that can be best seen at $\hbar\omega = 0.25$ meV in Fig. 2 (a). This mode is even more intense than the previously reported exciton at the R point, whereas its strong temperature dependence leaves no doubt about its magnetic origin. This new Γ-point mode is observed both at the (001) and (110) wave vectors, but its intensity apparently increases towards higher $|\mathbf{Q}|$, which makes it most pronounced at (110).

Next, we consider cuts through out dataset along several high-symmetry planes that are not parallel to the horizontal (HHL) plane. For example, Figs. 3 (a) and (b) show the intensity distribution in two planes orthogonal to the $\langle 111 \rangle$ diagonal of the cubic Brillouin zone and passing through the R and Γ points, respectively. They reveal a hexagonal arrangement of the spin-wave intensity from a sextet of S points near the R point. The spin wave intensity at the Σ point is much weaker and therefore can not be clearly seen. In Fig. 3(e), we also compare the intensity distributions in the $(\frac{1}{2}\,K\,L)$ plane (Brillouin zone face) passing through two R points at an energy transfer of 0.5 meV at both temperatures. Here we observe a similar elliptical feature around the M point as in the (HHL) plane, but the gaps separating it from the exciton mode at R become more obvious. At even lower energies (not shown) the intensity of the ellipse can be tracked down continuously to the spin-wave branches stemming from S and S'.

So far we have only considered constant-energy cuts through our data. Further insight can be obtained also by plotting momentum-energy cuts along certain high-symmetry directions of the reciprocal space. Several examples of such cuts are shown in Figs. 4 and 5. Along with the data measured at two temperatures below and above T_N, we also show the difference of the two datasets, which illustrates the redistribution of the magnetic spectral weight. Negative values (blue) correspond to the spin-gap regions, whereas positive values (red) signal the accumulation of spectral weight below T_N and the formation of various collective modes. In panels (a)–(c), one can see a pair of resonant modes at 0.5 meV in two equivalent R points,

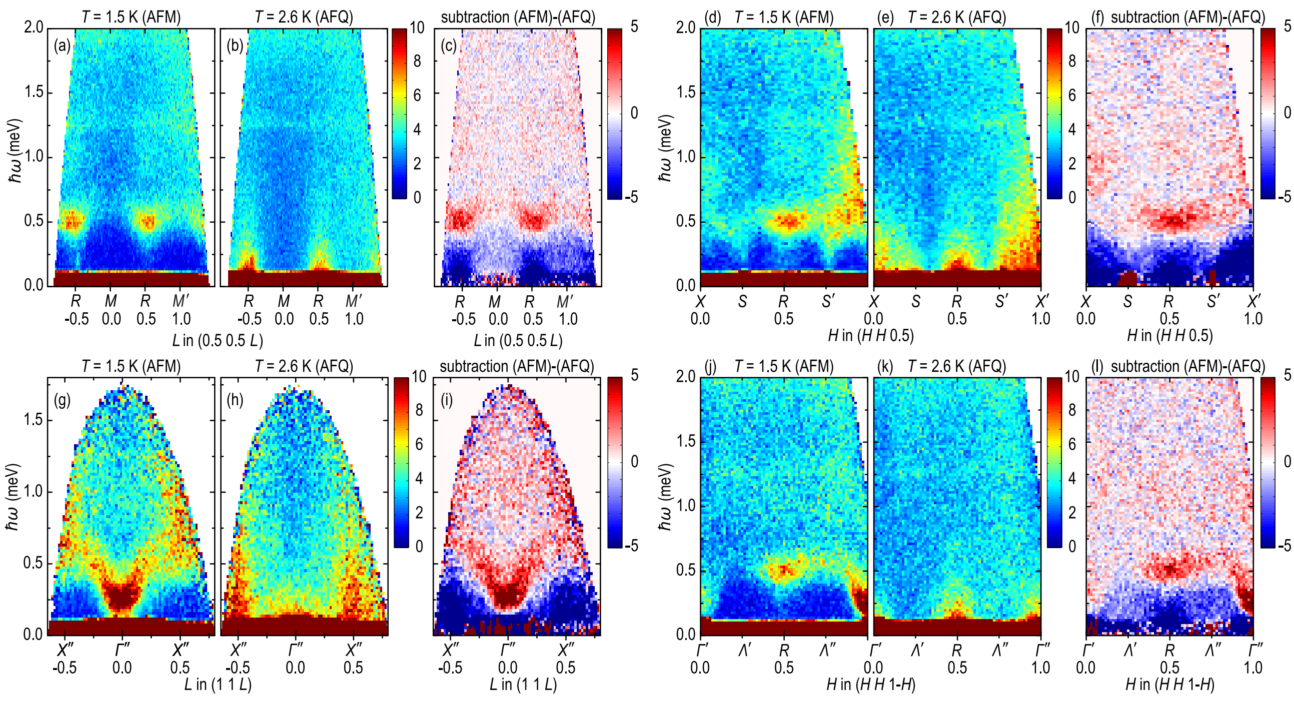

Fig. 4: Several representative momentum-energy cuts in the AFM and AFQ phases and their subtractions: (a)–(c) $(\frac{1}{2}\,\frac{1}{2}\,L)$ direction; (d)–(f) $(H\,H\,\frac{1}{2})$ direction; (g)–(i) $(1\,1\,L)$ direction; (j)–(l) $(H\,H\,1{-}H)$ direction.

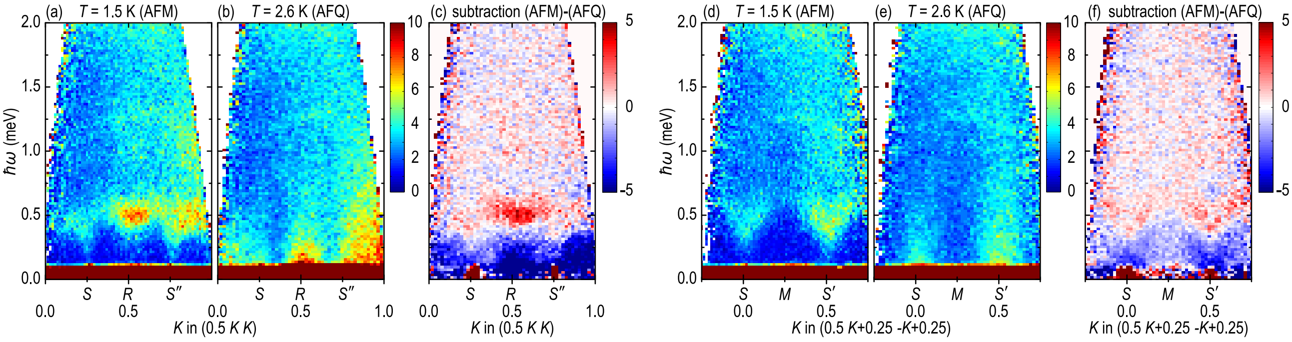

Fig. 5: Momentum-energy cuts, continued from Fig. 4: (a)–(c) $(\frac{1}{2}\,K\,K)$ direction; (d)-(f) $(\frac{1}{2}\;\frac{1}{4}{+}K\;\frac{1}{4}{-}K)$ direction.

reported in our earlier work [6]. We observe a weak dispersion of these modes towards higher energies ($\sim$0.7 meV). In panels (d)–(f) we can also see how they hybridize with the spin-wave cones emanating from the neighboring S points. A second broader peak of intensity at the R point is seen near $\hbar\omega = 1.1$ meV, as already reported [6], and vanishes above T_N. The previously discovered broad mode at the X point, centered around 0.9 meV [6], can also be clearly seen.

Figs. 4 (g)–(i) illustrate our most striking finding, namely the intense mode at the Γ point, which might be indicative of low-energy ferromagnetic correlations in CeB_6 [8–10]. This mode is centered at 0.25 meV and has a pronounced dispersion towards higher energies, reaching $\sim$0.7 meV at the zone boundary. In Figs. 4 (g)–(i), we can see that this ferromagnetic mode is connected continuously with the lower-energy part of the X-point feature, whereas in panels (j)–(l) of the same figure we observe a hybridization of this mode with the R-point exciton. Here the exciton at the R point appears as an intensity swelling near the zone boundary at the top of a dispersive branch emanating from Γ, which is in addition softened in energy. This results in an unusual $\mathcal{M}$-shaped dispersion along the Γ–R–Γ direction with a local maximum of intensity at R.

In Fig. 5, we additionally show a $(\frac{1}{2}KK)$ cut centered at the R point, which is equivalent to the one in Figs. 4 (d)–(f), and an S–M–S' cut that reveals two spin-wave branches at the AFM wave vectors above a spin gap of $\sim$0.3 meV. The top of the spin-wave dispersion is found near 0.7 meV at the zone boundary. The inelastic intensity distribution along all high-symmetry directions is also summarized in Fig. 6. Note that in all cuts presented in Figs. 4 – 6, the intensity becomes quasielastic above T_N, while its momentum structure is retained. This clearly excludes any dispersive modes in the AFQ state in zero magnetic field, which were previously suggested both theoretically [11] and experimentally [12].

Summary and discussion

In the present experiment, we obtained complete maps of the 4D energy-momentum space of CeB_6 in the AFM and AFQ states. Apart from identifying the origin of the elliptical feature surrounding the M point, which we now associate with the top of the spin-wave branches, we have also discovered an intense dispersive excitation centered at the Γ point, which has not been reported previously. Although the microscopic origin of this mode still remains a mystery, it is most likely associated with low-energy ferromagnetic fluctuations, presumably with a multipolar character, as they exhibit an anomalous enhancement of the magnetic form factor towards higher $|\mathbf{Q}|$. The presence of ferromagnetic correlations in CeB_6 has already been noted previously in several works [8–10], yet our measurements provide the first clear-cut observation of their characteristic energy scale, dispersion, and their relationship to other types of collective excitations, such as the previously found exciton mode at the R point.

The absence of any dispersive modes in the AFQ state and the apparent hybridization of the strong modes at the R and Γ points with the conventional spin-wave branches below T_N strongly suggests that any proper theoretical description of magnetic excitations in CeB_6 should take full account of both AFM and AFQ order parameters. Existing calculations [13] are presented in the folded magnetic Brillouin zone and therefore cannot be directly compared with our data without proper unfolding. Moreover, the itinerant flavor of the excitonic modes suggested by a recent theory [14] is not taken into account in these earlier models. Further theoretical developments addressing the rich interplay of different order parameters in CeB_6 would be therefore highly desirable.

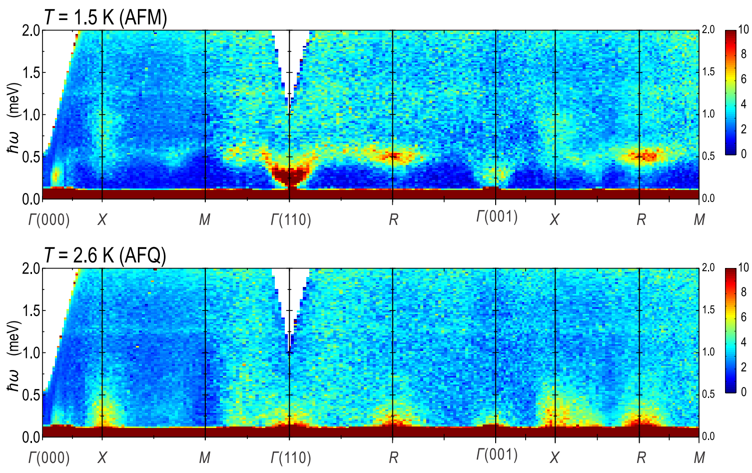

Fig. 6: Momentum-energy cuts along a polygonal path following high-symmetry directions in $\mathbf{Q}$-space for the AFM (top) and AFQ (bottom) states.

[1] J. M. Effantin *et al.*, JMMM **47–48**, 145 (1985).
[2] H. Nakao *et al.*, JPSJ **70**, 1857 (2001).
[3] T. Matsumura *et al.*, PRL **103**, 017203 (2009).
[4] S. Horn *et al.*, Z. Phys. B **42**, 125 (1981).
[5] V. P. Plakhty *et al.*, PRB **71**, 100407(R) (2005).
[6] G. Friemel *et al.*, Nature Communs. **3**, 830 (2012).
[7] ILL Experimental Report 4-01-912.
[8] S. Horn *et al.*, Z. Phys. B **42**, 125 (1981).
[9] N. E. Sluchanko *et al.*, JETP Lett. **88**, 318 (2008).
[10] S. V. Demishev *et al.*, Phys. Rev. B **80**, 245106 (2009).
[11] P. Thalmeier *et al.*, JPSJ **72**, 3219 (2003).
[12] A. Bouvet, PhD thesis (Grenoble, 1993).
[13] H. Kusunose and Y. Kuramoto, JPSJ **70**, 1751 (2001).
[14] A. Akbari and P. Thalmeier, PRL **108**, 146403 (2012).